


Article

Influence of an Electronic Structure of N-TiO₂ on Its Photocatalytic Activity towards Decomposition of Acetaldehyde under UV and Fluorescent Lamps Irradiation

Beata Tryba ^{1,*} , Magdalena Wozniak ¹, Grzegorz Zolnierkiewicz ², Nikos Guskos ², Antoni Morawski ¹, Christophe Colbeau-Justin ³, Rafał Wrobel ¹, Akio Nitta ⁴ and Bunsho Ohtani ^{4,5}

¹ Institute of Chemical Technology and Environment Engineering, West Pomeranian University of Technology, ul. Pułaskiego 10, 70-322 Szczecin, Poland; magdalena.tygielska@zut.edu.pl (M.W.); amor@zut.edu.pl (A.M.); rafal.wrobel@zut.edu.pl (R.W.)

² Institute of Physics, West Pomeranian University of Technology, Al. Piastów 17, 70-310 Szczecin, Poland; Nikos.Guskos@zut.edu.pl (N.G.); grzegorz.zolnierkiewicz@zut.edu.pl (G.Z.)

³ Laboratoire de Chimie Physique, CNRS UMR 8000, Univ Paris-Sud - Université Paris-Saclay, 91405 Orsay, France; christophe.colbeau-justin@u-psud.fr

⁴ Graduate School of Environmental Science, Hokkaido University, Sapporo 060-0810, Japan; nitta-salut-akio@cat.hokudai.ac.jp (A.N.); ohtani@cat.hokudai.ac.jp (B.O.)

⁵ Institute for Catalysis, Hokkaido University, Sapporo 001-0021, Japan

* Correspondence: beata.tryba@zut.edu.pl; Tel.: +48-609-573-930

Received: 3 January 2018; Accepted: 17 February 2018; Published: 20 February 2018

Abstract: The electronic structure of N-TiO₂ samples prepared by a sol-gel method was investigated by EPR (Electronic Paramagnetic Resonance) measurements and the energy-resolved distribution of electron traps. In EPR spectra, some of the resonance lines assigned to paramagnetic species of nitrogen and Ti³⁺ were detected. Sample prepared at 300 °C revealed the highest intensity line of the nitrogen paramagnetic centers, whereas that prepared at 400 °C showed a paramagnetic line for Ti³⁺. Measurements of the electron trap distribution showed higher density of electron traps for sample prepared at 400 °C than that at 300 °C. Sample prepared at 300 °C, which revealed the highest amount of nitrogen built in the titania in the interstitial position was the most active under visible light. It was evidenced that photocatalytic decomposition of acetaldehyde was dependent strongly on the BET surface area and electrokinetic potential of the photocatalyst surface. The UV content in the fluorescent lamp affected the yield of acetaldehyde decomposition.

Keywords: N-TiO₂; sol-gel; Electronic Paramagnetic Resonance (EPR); electron-trap distribution; photocatalytic properties

1. Introduction

Nitrogen-modified titania powders have been widely described in the literature as visible-light active photocatalysts, which can be used in different areas, such as: air and water purification and deactivation of microorganisms [1–7]. It has already been reported that visible light activity of N-TiO₂ depends on the concentration and way of incorporation of nitrogen species to TiO₂ and also concentration of oxygen vacancies [1,5,6]. Nitrogen can be built to titania at the oxygen lattice site or at the interstitial position [8,9]. Some researchers reported that at low concentrations of nitrogen dopant, such as 0.1 at.%, interstitial incorporation in titania occurred together with formation of oxygen vacancies. Such incorporation of nitrogen to TiO₂ enhanced its visible light activity. Contrary to that,

at higher levels of nitrogen incorporation in titanium dioxide, substitutional doping occurs together with lowering concentrations of oxygen vacancies [6]. Other scientists reported that visible light activity of N-doped TiO_2 was caused by the substitution of high concentration of nitrogen with the lattice oxygen atoms in TiO_2 [5]. Such substitution resulted in the narrowing of the band gap in TiO_2 . Thus, a controversy still remains regarding the way of nitrogen doping to titania and its electronic structure. Asahi et al. [10] and Irie et al. [11] explained the visible light activity of N-doped TiO_2 based on the performed density state calculations. They proposed a mechanism in which nitrogen atoms substituted oxygen atoms in the anatase type of TiO_2 . As a consequence, mixing of O 2p and N 2p state occurred and narrowing of the titania band gap was observed. However, Diwald et al. denied this thesis [12]. Di Valentin et al. [13] introduced also some doubts about mechanism of nitrogen doping proposed by Asahi and Irie. They did some experiments on nitrogen doping and proved, that by substitutional doping of nitrogen to TiO_2 some localized impurity states are formed just above the valence band of TiO_2 without mixing of N 2p and O 2p states. Nitrogen was also built to titania lattice in an interstitial position and formed localized energy levels in the form of NO bonds. Narrowing of the band gap was not observed, but such doping of nitrogen to TiO_2 caused its activity in the visible light [13]. Other researchers reported that absorption of visible light can be caused by oxygen vacancies, which are stabilized by doping of nitrogen [14]. Stabilization of oxygen vacancies is obtained due to the electron transfer between high energy Ti^{3+} states to the low-lying N states. The EPR technique seems to be very adequate to measure the localized magnetic moments and visible-light activity of N-doped TiO_2 . Meronia et al. [2] and Sakatani et al. [15] revealed that the concentration of paramagnetic centers in nitrogen-doped TiO_2 seemed to control the absorption of visible light and the activity of titania samples. Based on the knowledge that both oxygen vacancies and/or nitrogen paramagnetic defects located in the bulk of the N- TiO_2 nanocrystals can affect the visible light activity, some EPR measurements were performed in the prepared nitrogen-modified TiO_2 samples and the electronic structure of samples was discussed in relation to their visible light activities. Measurements of electron trap density were also performed according to a method described elsewhere [16].

The substitution of nitrogen in TiO_2 lattice depends on the preparation method and source of nitrogen. Plasma-enhanced chemical vapor deposition or RF (Radio Frequency) magnetron sputtering technique was conducted to substitutional doping of nitrogen, in contrast to the sol-gel method or annealing in NH_3 , which often results in doping of nitrogen predominantly at the interstitial position [1]. Here we are presented with a sol-gel method preparation of N-doped TiO_2 with following calcination at low temperatures. Influence of nitrogen doping at the different positions and the presence of reduced titania with oxygen vacancies on the photocatalytic activity under visible and UV lights will be discussed. Activity of the prepared N-doped TiO_2 photocatalysts for decomposition of acetaldehyde under irradiation of UV and fluorescent lamps was measured and compared with the reference samples prepared by the same sol-gel method but without nitrogen doping.

2. Results

2.1. Visible Light Activity of N-Doped TiO_2

Photocatalytic activity of N-doped TiO_2 samples under visible light was tested using reactions with terephthalic acid solution. Terephthalic acid (TA) readily reacts with hydroxyl radicals, which are formed on the surface of excited photocatalysts to form 2-hydroxyterephthalic acid (2-HTA) as a main product of the reaction, which can be easily determined by fluorescence spectroscopy. In this experiment, halogen lamp was used with a UV cut off filter ($\lambda > 425 \text{ nm}$). In Figure 1, the yield in formation of 2-HTA at the presence of photocatalysts and visible light irradiation was illustrated. For comparison, TiO_2 reference samples without nitrogen doping were also tested.

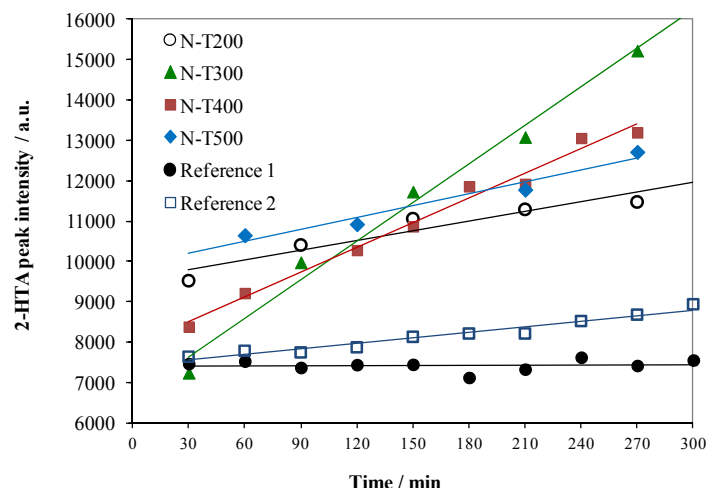


Figure 1. Formation of 2-HTA at the presence of N-TiO₂ and reference samples upon time of visible light irradiation.

Formation of 2-HTA was the most efficient at the presence of N-T300 sample. The Reference 1 sample did not show any activity and Reference 2 was somewhat active, but this activity could be negligible by comparison with the other samples. The k coefficient determined from the sloping of the fitting trend line was as follows: 8.0; 31.8; 22.0; 13.5; 0.1 and 4.6 for N-T200, N-T300, N-T400, N-T500, Reference 1 and Reference 2 samples, respectively.

2.2. Photocatalytic Decomposition of Acetaldehyde on N-TiO₂ Samples

In Figure 2, photocatalytic decomposition of acetaldehyde under fluorescent lamp irradiation is presented. This light contained visible light with a share of UV-A. The rate of acetaldehyde decomposition was dependent on the flow rate of acetaldehyde gas through the reactor; the slower the flow rate the higher the decomposition. The selected speed of gas flow was 5 mL/min.

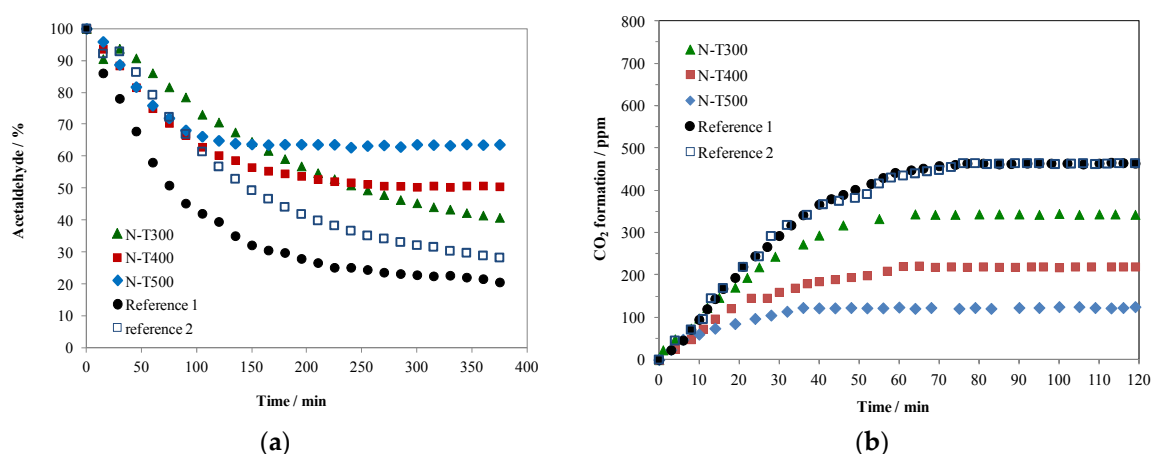


Figure 2. Photocatalytic decomposition of acetaldehyde on N-TiO₂ and reference samples under fluorescent lamp irradiation, (a) changes in acetaldehyde concentration; (b) formation of CO₂ upon acetaldehyde decomposition.

All the N-doped TiO₂ samples showed lower activity towards acetaldehyde decomposition by comparison to undoped TiO₂. Among all the prepared N-TiO₂, the one calcinated at 300 °C was the most active. Both reference TiO₂ samples showed the same degree of acetaldehyde mineralisation, however, Reference 1 exposed higher conversion of acetaldehyde than Reference 2. Taking into account

that the total decomposition of acetaldehyde in the concentration of 300 ppm gives 600 ppm of CO_2 , it was calculated that the amount of acetaldehyde decomposition towards CO_2 was equal to 77, 57, 37 and 24% for reference samples N-T300, N-T400, and N-T500, respectively. Although the fluorescent lamp contains a large region in the visible spectrum, the presence even of a small part of UV light caused TiO_2 samples which did not have any significant visible light activity to be very active. The performed blank test of acetaldehyde decomposition in an empty reactor irradiated by a fluorescent lamp showed that 8.5% of acetaldehyde gas was totally decomposed. This test showed clearly that UV activity of TiO_2 was much more powerful than the visible one. For comparison, activity of the prepared N- TiO_2 and reference samples towards acetaldehyde decomposition under UV light irradiation was tested and the results are illustrated in Figure 3.

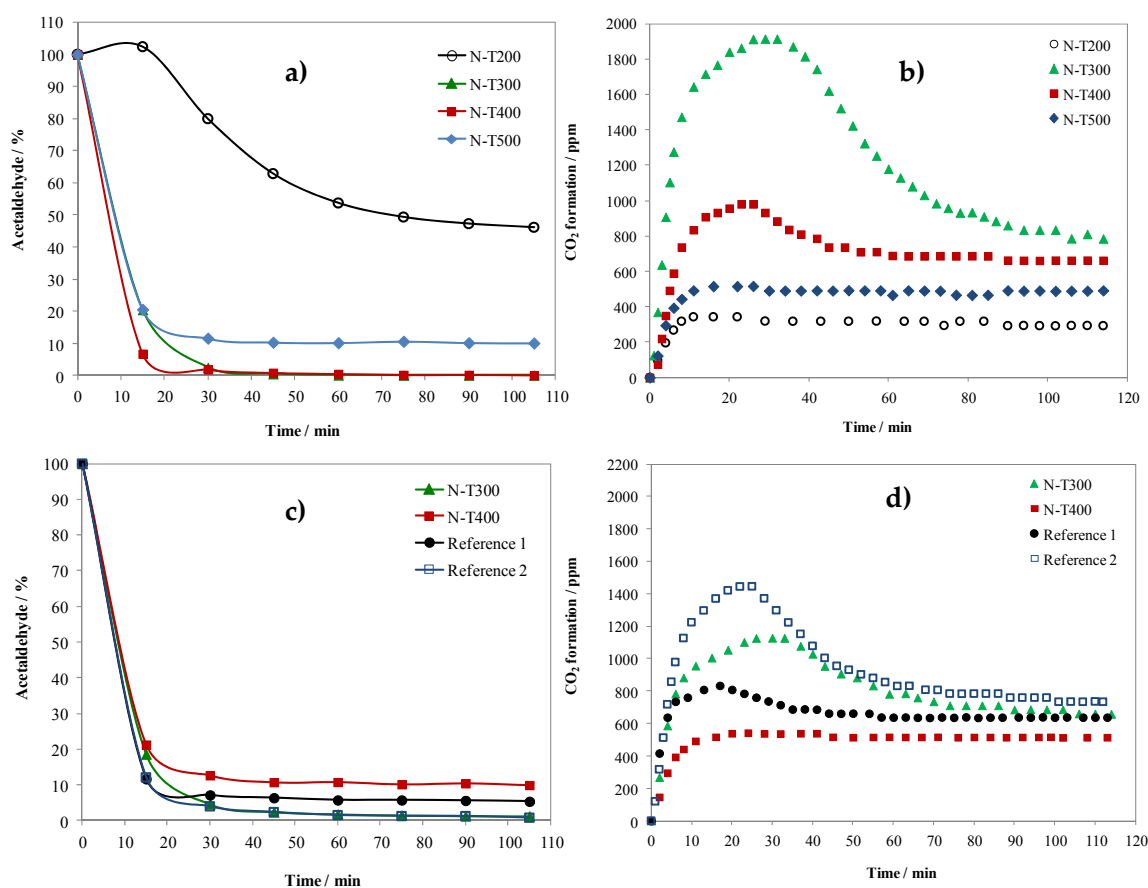


Figure 3. Photocatalytic decomposition of acetaldehyde on N- TiO_2 and reference samples under UV light, (a) and (c) changes in acetaldehyde concentration (sample surface = 24 cm² and 12 cm², respectively), (b) and (d) formation of CO_2 (sample surface = 24 cm² and 12 cm², respectively).

From Figure 3a it can be seen that samples prepared at 300 and 400 °C were the most active, whereas that prepared at 200 °C, which was not totally crystallized due to the low temperature of calcination, showed the lowest activity. Acetaldehyde decomposition on samples N-T300 and N-T400 was repeated but for the reduced surface (3 plates—12 cm²) in order to determine which one was more active. The reference samples were also tested using three plates of sample coatings. The results are illustrated in Figure 3c. This experiment showed clearly that the sample prepared at 300 °C was more active under UV light than that obtained at 400 °C. The Reference 2 sample had a comparable activity with N-T300, but both reference samples were more active than N-T400.

CO_2 formation during acetaldehyde decomposition is illustrated in Figure 3b,d. It can be seen that the amount of CO_2 at the beginning of irradiation was increasing and then stabilized. This

phenomenon was observed especially in the samples which showed the highest decomposition rate of acetaldehyde. It is assumed that the excess of formed CO_2 at the beginning of the process was caused by the decomposition of preliminary adsorbed acetaldehyde (due to the heating of the UV lamp). So, it is deduced that samples which revealed the formation of a high quantity of CO_2 at the beginning were good adsorbents for acetaldehyde. High BET surface area and high affinity of photocatalyst surface to adsorption of acetaldehyde could be the main factors determining their photocatalytic performance.

2.3. Characteristics of N-TiO₂ Photocatalysts

In Figure 4, XRD patterns of N-TiO₂ and reference samples were illustrated.

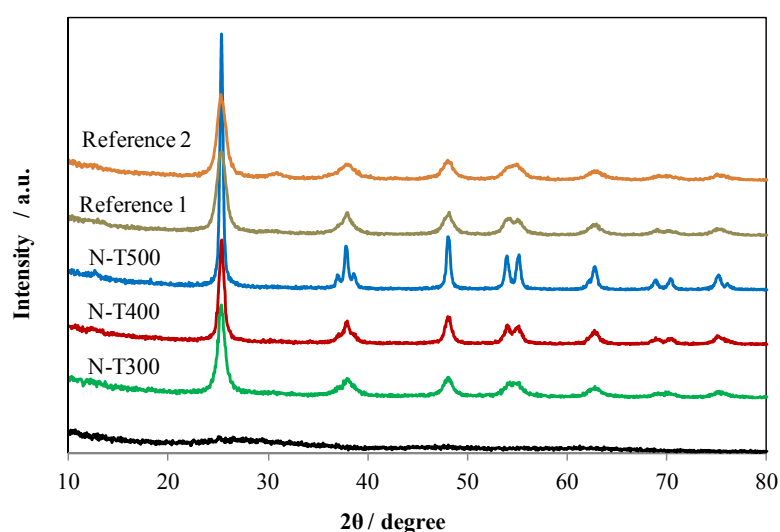


Figure 4. XRD patterns of N-TiO₂ and reference samples.

XRD analyses showed that the N-TiO₂ sample calcinated at 200 °C was amorphous and those that were heat-treated at 300–500 °C had a single anatase phase. Crystallinity was increasing with increased temperature of calcination. The Reference 1 sample was a single anatase phase, whereas Reference 2 consisted of anatase and brookite. The reflex of brookite was visible at the 2 θ of around 30°. Both reference samples were obtained by a sol-gel preparation and further calcination at 400 °C, however, the N-T400 sample revealed higher crystallinity than the reference ones. The phase composition and crystallites size calculated from Scherrer equation are introduced in Table 1 together with other parameters of samples such as BET surface area and zeta potential.

Table 1. BET surface area, mean crystallites size and potential zeta of N-TiO₂ and reference samples.

Sample	HTT (°C)	BET (m ² /g)	Phase Composition	Mean Crystallites Size (nm)	Potential Zeta (mV)
N-T200	200	354	Amorphous	-	−23.0
N-T300	300	153	Anatase	11.6	−16.4
N-T400	400	50	Anatase	16.3	−21.4
N-T500	500	16	Anatase	34.1	−15.2
Reference 1	400	140	Anatase	8.7	−17.3
Reference 2	400	124	Anatase/Brookite = 0.87/0.13	A(16.2); B(8.1)	−15.4

All these samples showed acidic character of surface. The lowest value of negative potential zeta was noticed for amorphous TiO₂ and sample doped with nitrogen, calcinated at 400 °C. Anatase

crystallites were increasing with increase temperature of calcination. The lowest crystallites size of anatase had Reference 1 sample. The highest BET surface area among crystallised TiO_2 was noticed for N-T300.

The activity of N- TiO_2 samples under visible and UV light and the lifetime of charges after excitation with laser was measured by TRMC (Time Resolved Microwave Conductivity). For laser excitation, two wavelengths were selected, $\lambda = 460$ and 360 nm; the results are presented in Figure 5.

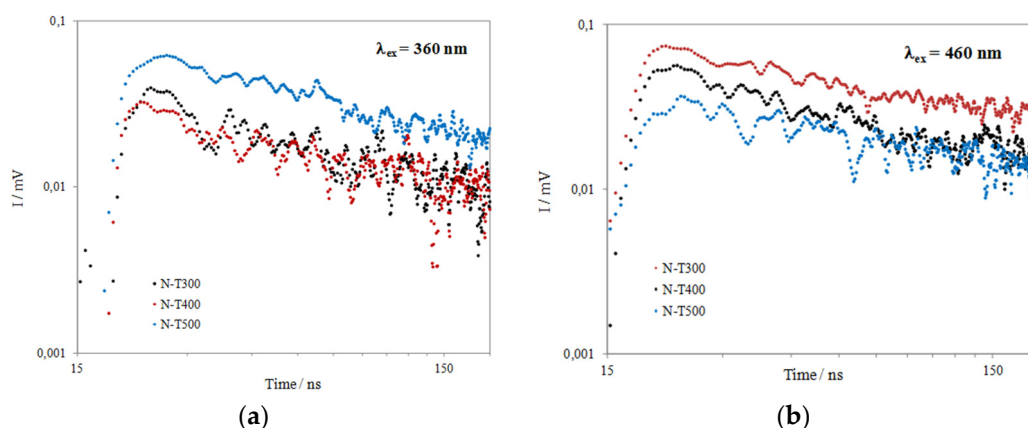


Figure 5. Decay of TRMC signals in N- TiO_2 samples prepared at 300–500 °C, (a) excitation at $\lambda = 360$ nm and (b) 460 nm.

Sample N-T200 was not included, because it was amorphous and did not show any TRMC profile. Some parameters such as maximal intensity of TRMC signal (I_{max}), intensity after 40 ns (I_{40}) and I_{40}/I_{max} ratio are introduced in Table 2.

Table 2. TRMC parameters for N- TiO_2 samples.

Sample	λ_{ex} (nm)	I_{max}	I_{40}	I_{40}/I_{max}
N-T300	460	0.074	0.043	0.58
N-T400	460	0.056	0.031	0.55
N-T500	460	0.039	0.026	0.67
N-T300	360	0.039	0.020	0.51
N-T400	360	0.032	0.013	0.41
N-T500	360	0.062	0.040	0.65

The short-range decay was set to 40 ns after the maximum of the pulse was reached, and is expressed as the I_{40}/I_{max} ratio, which represents the fast processes occurring during and just after the pulse. The fast decay in this short range is caused mostly by an electron-hole recombination and scavenging of electrons, which can also occur. Similar analyses of TRMC signals were performed and published elsewhere [17,18]. It can be observed, that under laser excitation at $\lambda = 360$ nm, N- TiO_2 prepared at 500 °C showed the highest TRMC signal and at the same time the lowest one under excitation at $\lambda = 460$ nm. It can be deduced that this sample can have high photocatalytic activity under UV and low activity under visible light irradiation, by comparison with the others. TRMC short range decay (I_{40}/I_{max}) had the highest value for the N-T500 sample which means that this represents the longest lifetime of free charges, caused probably by its high size of anatase crystallites. Sample prepared at 300 °C showed longer lifetime of free charges than for the heat-treated one (at 400 °C) and also the highest TRMC signal under visible light excitation. This means that this sample (N-T300) can exhibit the highest activity under visible light among all the other samples and its activity under UV light can be higher than for N-T400.

Figure 6 shows the EPR spectra at $T = 4$ K performed for N-TiO₂ nanocomposites obtained with different thermal treatment processes.

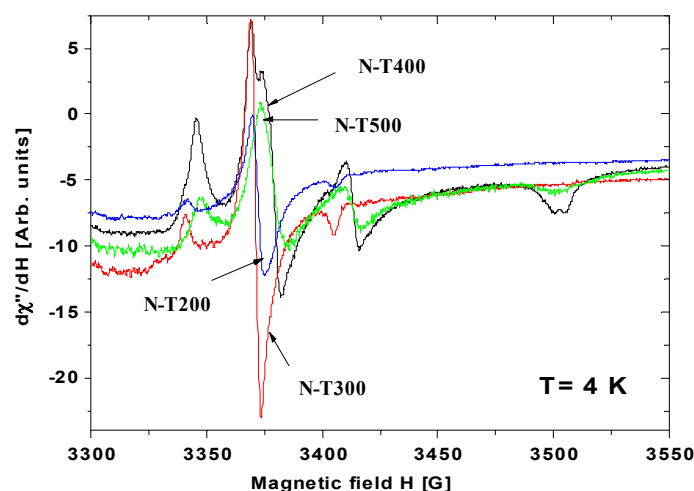


Figure 6. EPR spectra of localized magnetic centers for N-TiO₂ samples prepared at 200–500 °C performed at temperature $T = 4$ K.

For samples heat treated at 200 and 300 °C, some of the resonance lines centered at $g = 1.985$, $g = 2.003$, $g = 2.023$ are seen. They can be related to the paramagnetic nitrogen centers ($g = 2.003$) and oxygen vacancies (Ti^{3+} in hydrated titania), $g = 2.023$ and $g = 1.985$. They are more intensive in N-T300 than in N-T200. In the sample calcinated at 400 °C, there are still signals from paramagnetic nitrogen and oxygen vacancies, however, less intensive than in the sample prepared at 300 °C and additional resonance lines appear at $g = 2.02$, $g = 2.001$, $g = 1.98$ and $g = 1.93$. Sample N-T500 showed resonance lines at $g = 2.02$, $g = 2.001$, $g = 1.98$ and $g = 1.93$, but these were less intensive than sample N-T400. At higher temperatures of calcination, oxygen vacancies disappear. Samples prepared at 500 °C showed less defected structure than the others. The presence of oxygen vacancies for primary particle sizes below ca. 20 nm is typical and have been already reported in the literature [9]. High intensity of resonance lines related to paramagnetic nitrogen in N-T300 sample can explain why this sample generated the highest amount of free charges under visible light. Meroni et al. [2] noticed the highest activity of N-doped sample under solar light irradiation, which showed the largest amount of paramagnetic nitrogen species.

The amounts of nitrogen and carbon in the bulk titania samples were measured in CN628 elemental analyzer; the results are listed in Table 3.

Table 3. Content of carbon and nitrogen in the prepared N-TiO₂ and reference samples.

Sample	N (%)	C (%)
N-T200	0.6	0.3
N-T300	0.1	0.08
N-T400	0.07	0
N-T500	0	0
Reference 1	0	0
Reference 2	0	0

The sample prepared at 200 °C showed the highest quantity of both, nitrogen and carbon. For higher temperature of calcination, lower amounts of nitrogen and carbon were present in the samples. In N-T500 sample, both nitrogen and carbon were out of the detection limit. The sample calcinated at 200 °C showed higher content of nitrogen, but lower EPR signal related to the

paramagnetic nitrogen. It is suggested that in this sample, some of the nitrogen species were physically adsorbed on the titania surface. The reference samples did not contain any carbon and nitrogen.

FTIR measurements were performed to determine the presence of functional groups on the nitrogen-modified TiO_2 surface. In Figure 7, FTIR spectra of the prepared N- TiO_2 samples are presented.

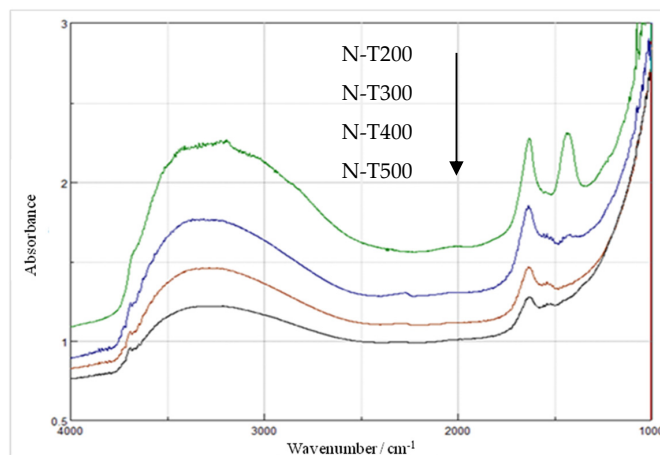


Figure 7. FTIR spectra of N- TiO_2 samples prepared at 200–400 °C.

All the FTIR spectra showed characteristic bands for OH groups at: $1630\text{--}1620\text{ cm}^{-1}$, $3700\text{--}2600\text{ cm}^{-1}$, and 3700 cm^{-1} . The broad band at $3700\text{--}2600\text{ cm}^{-1}$ is due to the stretching vibrations of adsorbed water and hydrogen-bonded hydroxyl groups. The band at $1630\text{--}1620\text{ cm}^{-1}$ is characteristic of the bending mode of adsorbed water on titania surface and the band at 3700 cm^{-1} is assigned to hydroxyl groups bound to the surface of one Ti atom [19,20]. OH bands were significantly reduced upon calcination at higher temperatures due to the dehydration process. The broad and high intensive band at 1450 cm^{-1} is visible for sample prepared at 200 °C and can be assigned to vibrations of the Ti-N bond [20]. The intensity of this band was reduced after calcination at 300 °C and disappeared in samples heat-treated at higher temperatures. The band at 1532 cm^{-1} is assigned to the stretching vibrations of titanium carboxylate. Carboxylate groups on the TiO_2 surface could be formed from ethanol and TIP used during titania preparation.

The presence of nitrogen groups in TiO_2 can give response of titania in the visible region, therefore, some of UV-Vis/DR measurements were performed and recorded spectra are illustrated in Figure 8.

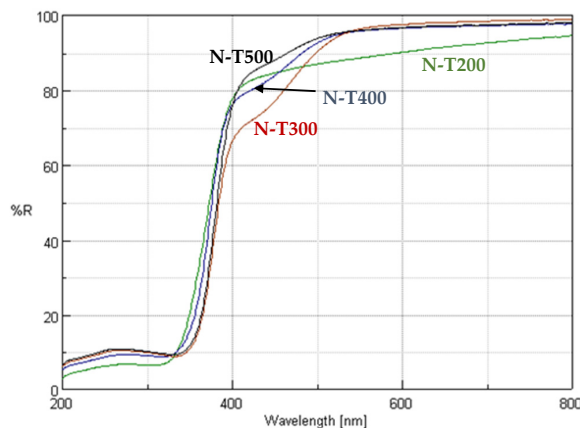


Figure 8. UV-Vis/DR spectra of N- TiO_2 samples prepared at 200–400 °C.

Samples prepared at 200 °C showed absorption in all the range of visible light, but samples heat-treated at 300–500 °C showed significant absorption at the range of around 400–520 nm, which was attributed to the building of nitrogen to the titania lattice. It is worth noting that the N-T300 sample, which revealed the highest intensity of resonance line related to the paramagnetic nitrogen, showed also the highest intensity of absorption peak at the range of 400–520 nm. In order to determine the energy of the band gap, the function of Kubelka–Munk was applied for semiconductors with indirect allowed transition. This method was described in detail elsewhere [21]. The plots of Kubelka–Munk transformation versus E_g for N-TiO₂ samples together with calculated E_g values are introduced in Figure 9.

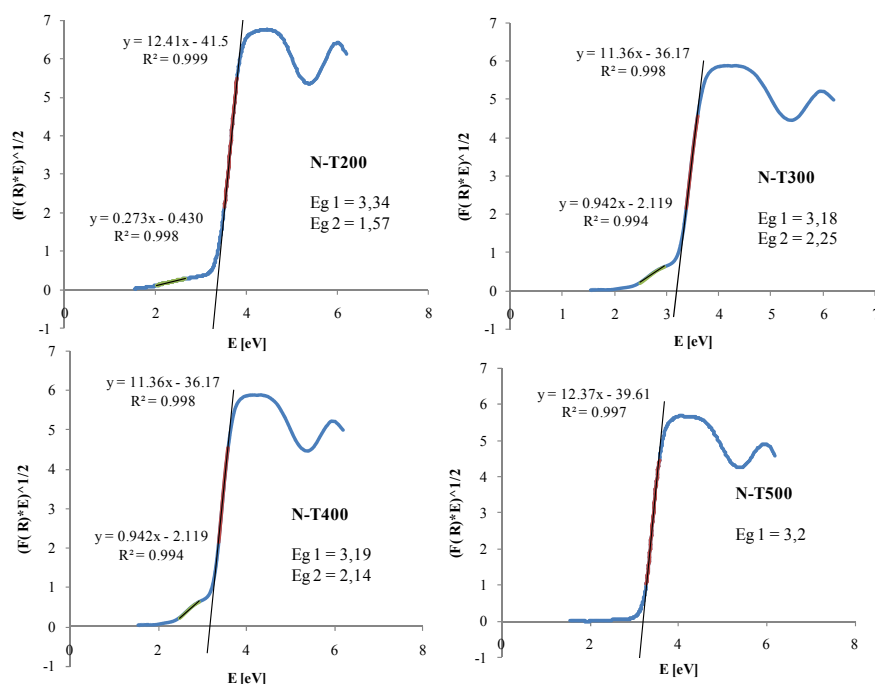


Figure 9. Plots of modified Kubelka–Munk: $(F(R)hv)^{1/2}$ versus E_g for N-TiO₂ samples.

For sample N-T500, one value of E_g was determined. Sample N-T200, which consisted of small size particles had a higher value of E_g than the other samples, which is typical in case of nanoparticles. For samples N-T200, N-T300 and N-T400, two values of E_g were calculated, one in the UV and the second in the visible region. This suggests formation of a midgap inside of the E_g of titania sample.

XPS measurements were performed to identify the structure of nitrogen doped to TiO₂. XPS spectra of the prepared N-TiO₂ samples are presented in Figure 10 and the elemental composition of the surface in Table 4.

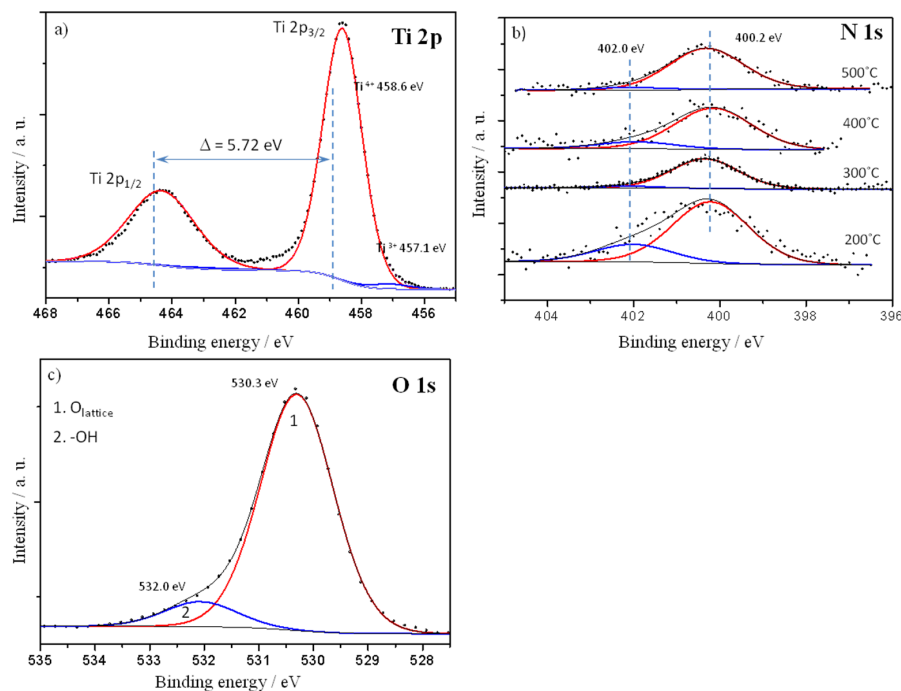


Figure 10. Deconvoluted XPS spectra; (a) Ti 2p signal of N-T300 sample; (b) N 1s signals of all the prepared samples; (c) O 1s signal of N-T300 sample.

Table 4. Elemental composition of the surface (by XPS).

Sample	Ti (at.%)	O (at.%)	N (at.%)
N-T200	23.2	75.5	1.4
N-T300	26.1	73.5	0.4
N-T400	25.3	74.0	0.7
N-T500	23.1	76.5	0.5

The restrictions for parameters of the Ti 2p fitting model were set [22]. The energy difference of Ti^{3+} and Ti^{4+} signals was 1.5 eV. The intensity ratio of the doublet components i.e., $\text{Ti } 2p_{3/2}$ and $\text{Ti } 2p_{1/2}$ was 2:1, respectively. The separation of Ti 2p doublet signal was set to be 5.73 eV. The transitions of the same kind were forced to have the same full width at half maximum (FWHM) e.g., $\text{Ti } 2p_{3/2}$ had the same FWHM for Ti^{4+} and Ti^{3+} but different for $\text{Ti } 2p_{1/2}$. The sample charge was calibrated according to $\text{Ti}^{4+} 2p_{3/2}$ transition at 458.6 eV. The O 1s signal was deconvoluted for two components at 530.3 eV and at about 532.0 eV. These components were attributed to titania phase and OH groups on titania surface, respectively [23]. The FWHM of oxygen components was forced to be the same due to the same kind of transition. In Figure 10a, the Ti 2p XPS spectrum of the sample obtained at 300 °C is presented. The deconvolution of the spectrum enables the determination of Ti^{4+} and Ti^{3+} contents which are given in Table 5.

Table 5. Elemental composition of the surface (by XPS).

Sample	Ti 2p (%)		N 1s (%)		O 1s (%)	
	4 ⁺	3 ⁺	400.2 eV	402 eV	Surface	Lattice
N-T200	98	2	78	22	10	90
N-T300	98	2	94	6	10	91
N-T400	98	2	86	14	8	92
N-T500	99	1	94	6	7	94

In all samples, the content of Ti^{3+} is below 2% of all titanium atoms, therefore, all Ti 2p spectra look very similar. The same situation is in case of O 1s signals. This is why only one spectrum of the most photocatalytically active sample is presented.

In case of N 1s signal, it can be observed that surface nitrogen content is highest for the N-T200 sample (Table 4). The concentration values are consistent with works of other researchers where the nitrogen concentration is in the range of 0.15–2.0 at.% and decreases with increase of temperature of preparation [24–26]. In our experiments, the nitrogen concentration also decreases at higher temperatures which can be explained by thermal desorption of nitrogen species. It is consistent with elemental analysis. Interestingly, the sample prepared at 400 °C has higher surface nitrogen concentration compared to these obtained at 300 °C and 500 °C. Note that XPS delivers information about surface concentration. Therefore, a higher nitrogen concentration at 400 °C compared to that at 300 °C may be a result of thermal segregation of nitrogen from the bulk to the surface. At 500 °C, the bulk of the material is depleted from nitrogen as confirmed by elemental analysis (Table 3) which correlates with decrease of nitrogen surface concentration. Summarizing, there are two processes, i.e., segregation of nitrogen from the bulk to the surface followed by desorption of nitrogen species. Depending on the rate of these processes, which in turn are dependent on temperature, there is difference in the surface concentration of nitrogen.

Interestingly, the N 1s signal consists of two components at least. The one located at 400.2 eV is attributed to bulk nitrogen located in interstitial positions, thus, commonly named interstitial nitrogen [24]. The literature data gives the binding energy of such nitrogen at about 400 eV [24]. Nitrogen may also substitute oxygen in the lattice. However, in such position, the binding energy is lower, i.e., 396 eV [24]. In our measurements, we have not detected such nitrogen. There is lot of work indicating that interstitial nitrogen enhances the photocatalytic activity in visible light while the substitutional does not [24].

Nitrogen may be present also over the very surface as atomic nitrogen or in the form of a compound, e.g., NH_x , NO^{3-} , NO/ NO_2 [25,27]. These species exhibit banding energies of 400, 407.3 and 401.7 eV, respectively [25,27]. In our measurements, the N 1s signal was not symmetric and deconvolution reveals the presence of 402.0 eV component. We attribute this component to either atomic nitrogen over the titania surface or the species like NO or even N-C. Interestingly, in studies [27] and [28], the 400 eV N 1s signal is also asymmetric, however, the presence of higher binding energy component is not commented upon. In [26], the position of N 1s signal is 401 eV. Thermal treatment leads to significant narrowing of the signal FWHM (Full Width at Half Maximum). This indicates that in [26], there may be both 400 and 402 eV components interpreted erroneously as 401 eV signal. The literature data does not allow to uniquely determine the chemical nature of 402 eV nitrogen. Especially the oversimplification of the N-TiO₂ systems is observed, i.e., small numbers of possible bulk and surface species are assumed. However, the sample of the highest photocatalytic activity exhibited the lowest surface concentration of the 402.0 eV nitrogen.

Figure 11 shows ERDT (Energy-Resolved Distribution of electron Traps)/CBB (Conduction Band Bottom) patterns of N-TiO₂ samples prepared at 300 and 400 °C.

The CBB positions, reflecting the bulk (crystalline) structure, was slightly different; CBB positions of N-T300 and N-T400 were ca. 3.2 and 3.1 eV, respectively. The lower value of CBB for the latter sample could be caused by the formation of reduced titania below the conductive band. ERDT patterns of N-T400 contained deep (low energy) ETs at 2.7–2.8 eV in addition to the shallow (high energy = around CBB) ETs, while N-T300 did only shallow ETs. Although it is still speculative and there is no direct evidence obtained until now, shallow and deep ETs are beneficial and detrimental, respectively, due to promoted transfer of photoexcited electrons and enhanced recombination of an electron and a positive hole [29]. Higher temperature calcination at 400 °C might lead to formation of deep ETs leading to slight reduction of photocatalytic activity.

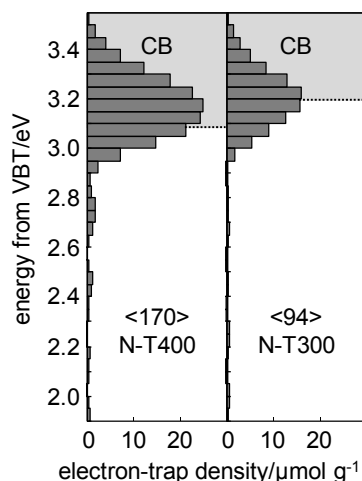


Figure 11. ERDT/CBB patterns of N-TiO₂ samples prepared at 300 and 400 °C (N-T300 and N-T400). Figures in <> denote total density of ETs (Electron Traps) in units of $\mu\text{mol}\cdot\text{g}^{-1}$.

3. Discussion

These measurements allowed to explain some doubts about visible light activity of N-TiO₂ and clearly showed that photocatalytic activity under visible light is caused by nitrogen doping in the interstitial position. Such built nitrogen species can be detected by EPR; higher concentration of the interstitial built nitrogen resulted in the higher intensity of the resonance line related to the nitrogen paramagnetic centers. The highest concentration of N doped to TiO₂ in the interstitial position was observed for the sample calcinated at 300 °C. Below this temperature, substitutional doping of nitrogen dominates and above this temperature segregation of nitrogen from the bulk to the surface occurs and reduces the amount of nitrogen doped at the interstitial position (as was evidenced by XPS). As a consequence, at 400 °C, some oxygen vacancies are formed together with Ti³⁺ species located at the bottom of the conductive band. The electronic structure of titania sample doped with nitrogen and calcinated at 400 °C exhibited higher density of electron traps than samples prepared at 300 °C, however, the latter one was the most active under visible light, as was demonstrated by conversion of HTA to 2-HTA at the presence of photocatalysts and formed OH radicals on their surface after excitation with visible light irradiation. In the photocatalytic decomposition of acetaldehyde under fluorescent lamp irradiation, the presence of UV light appeared to be very important and determined the rate of its decomposition. Therefore, the reference samples, which were very active towards acetaldehyde decomposition under UV light showed also high activity under fluorescent lamp irradiation; this activity was even higher than the activity of the N-T300 sample, which was the best among all the prepared N-doped TiO₂. It seems that activity of N-doped TiO₂ under visible light deteriorated their activity towards acetaldehyde decomposition at the presence of both, UV and visible lights. In fact, it was proved that in the aqueous medium, N-doped TiO₂ generated hydroxyl radicals under visible light. These radicals are formed by reaction of holes with hydroxyl ions in water. In a gas medium, acetaldehyde in a dry synthetic air was used, so formation of hydroxyl radicals on the surface of photocatalyst in such conditions was limited. Moreover, excitation of N-doped TiO₂ by visible light allows the transfer of electrons from the valence band to a nitrogen midgap. From transfer of electron from the midgap to the conductive band, there is need for another incident photon. The most probable reduction of oxygen with the excited electron occurs more favorably at the surface of the conductive band than at the midgap, because the conductive band has more negative potential than the other middle band gaps, which are placed between conductive and valence bands. So, some excited electrons from the valence band can migrate to midgap and if there is no reaction with adsorbed species, then they recombine with holes and deteriorate the photocatalytic process. Therefore, the quantum yield is decreasing in case of N-doped TiO₂ used under irradiation of a fluorescent

lamp. The photocatalytic tests of acetaldehyde decomposition showed that preliminary adsorption of acetaldehyde on the titania surface is very important. From these results, it was observed that high acidic surface was not favorable for acetaldehyde decomposition. Therefore, the presence of reduced titania did not enhance the photocatalytic activity of the sample due to increase of its hydrophilicity, which was the most probably disadvantage for adsorption of acetaldehyde. High BET surface area is also important for efficient degradation of acetaldehyde; for example sample N-T500 and Reference 2 had quite similar values of zeta potential but differ in the surface area; as a consequence their activity towards acetaldehyde degradation was extremely different. However, an amorphous structure of TiO_2 with relatively high BET surface area did not give any essential photocatalytic effect. Therefore, the most active samples should have well crystalized structures, relatively high BET surface area and high affinity of surface towards adsorbate, which undergoes photocatalytic decomposition.

4. Materials and Methods

4.1. Preparation of Nitrogen Modified TiO_2 Photocatalyst

N- TiO_2 photocatalyst was prepared by a sol-gel method from titanium (IV) isopropoxide, ($\geq 97\%$, Sigma-Aldrich Co., St. Louis, MI, USA) (TIP) and ammonia solution (25% pure, Avantor Performance Materials Poland S.A., (Gliwice, Poland) with addition of ethyl alcohol, $\geq 96\%$ (Chempur, Piekary Slaskie, Poland). At first, titanium precursor (20 mL) was mixed with 5 mL of ethyl alcohol under magnetic stirring and then 50 mL of ultrapure water was slowly added to this solution. After that ammonia water was added in the quantity allowing to obtain $\text{pH} = 10$. Such prepared mixture was magnetically stirred for 24 h and then left for the aging process taking one day. After that the obtained gel was dried in a drier at 100°C for 24 h and after grinding was subjected to calcination at various temperatures, from 200 to 500°C for 1 h. The Reference 1 and 2 samples were prepared according to the same procedure without addition of ammonia water; the Reference 1 was prepared with addition of acetic acid during hydrolysis to obtain pH of sol-gel solution equaled 3. Both reference samples were calcinated at 400°C in a muffle furnace for 1 h. Detailed characteristics of the reference samples was described in the previous paper [30].

4.2. Material Characteristics

Prepared N- TiO_2 samples were characterised by XRD, UV-Vis/DR, FTIR and EPR Spectroscopies, XPS, zeta potential, TRMC (Time Resolved Microwave Conductivity), BET measurements and new developed metod [16]—reversed double-beam photoacoustic spectroscopy (RDB-PAS) for ERDT (energy-resolved distribution of electron traps) measurements. The X-ray diffraction patterns were measured with X'Pert PRO diffractometer (ANalytical, Almelo, The Netherlands), using $\text{CuK}\alpha$ lamp ($\lambda = 1.54439 \text{ \AA}$, 35 kV, 30 mA). The sizes of the crystallites were calculated from the Scherrer's equation, based on the performed XRD measurements. BET surface area was determined from the measurements of nitrogen adsorption performed at 77 K in QUADRASORB Si analyzer (Quantachrome, FL, USA). Before these measurements the samples were followed the heating process at 105°C for 12 h under high vacuum to clean the surface from adsorbed gases. The optical parameters of N- TiO_2 samples were measured by using UV-Vis/DR spectroscopy in Jasco V-650 spectrophotometer. The energies of the band gap were determined from the conversion of the UV-Vis/DR spectra, by plotting of the Kubelka-Munka function, $(F(R)h\nu)^{1/2}$ versus $h\nu$, where R—reflectance, h —Planck constant, ν —frequency and $F(R) = (1-R)^2/2R$. This method is frequently used for semiconductors such as TiO_2 with indirect transition. FT-IR/DRS spectra were measured by using reflection technique in spectrophotometer FT/IR 4200 of Jasco Company (Tokyo, Japan). Spectra were measured with resolution of 4 cm^{-1} and a scanning speed of 1 mm/s . The background was recorded at the beginning of the measurements and was subtracted from the spectra of samples. The electrokinetic potential of photocatalysts particles surface was measured in Zetasizer Nano ZS analyzer of Malvern Company. For measurements samples were dispersed in a 1% of Triton solution, the non-ionic surfactant.

Every sample was measured at least 3 times and an average value was taken as a final result. The measurements of the EPR spectra were performed on a conventional X band ($\nu = 9.4$ GHz) Bruker E 500 spectrometer with 100 kHz magnetic field modulation. The measurements were performed at temperature of 4 K using an Oxford helium flow cryostat. Lifetime of charge carriers formed after excitation of N-TiO₂ samples with laser was measured by TRMC method, which was invented by C. Colbeau-Justin and described in the previous paper [17]. This method is based on the measurement of the change of microwave power reflected by the sample after inducing it by the laser pulse. The samples were analyzed in the form of powders. The microwaves were generated by means of a Gunn diode in the K α band (28–38 GHz). All experiments were carried out at 31.4 GHz. The reflected microwaves were detected by a Schottky diode. The emitted signal was amplified and displayed on a digitizer. The pulsed light source was an OPO laser (EKSPLA, NT342B) tunable from 225 to 2000 nm. It delivers 8-ns FWHM pulses with a frequency of 10 Hz. The measurements were carried out under both, UV (360 nm) and visible (460 nm) light irradiations. The maximum light energy, which was received by the sample was $1.5 \text{ mJ}\cdot\text{cm}^{-2}$ for the UV and $6.4 \text{ mJ}\cdot\text{cm}^{-2}$ for visible light. Analyses of carbon and nitrogen contents in samples were performed with using CN628 elemental analyzer (LECO Corporation, St. Joseph, MI, USA). The certified EDTA standard (LECO Corporation, St. Joseph, MI, USA) containing 41.06 ± 0.09 wt.% of carbon and 9.56 ± 0.03 wt.% of nitrogen was used for preparation of a calibration curve.

The X-ray photoelectron spectroscopy measurements were performed in a multipurpose (XPS, LEED, UPS, AES) UHV system (PREVAC, Rogów, Poland). The calibration of spectrometer was performed using Ag 3d_{5/2} transition. XPS measurements were performed under vacuum at the range of 9–10 mbar after degassing of sample at the first stage. The X-ray photoelectron spectroscopy was performed using Al K α ($h\nu = 1486.6$ eV) radiation. The measurements were performed for binding energies corresponding to Ti 2p, O 1s, N 1s regions. Results were elaborated with using the CasaXPS version 2.3.16 Dev 39.

The ERDT measurement by RDB-PAS is a newly developed technique for characterization of powdery metal-oxide samples which have “electron traps” (ETs) to accept electrons. As reported previously [16], energy of ETs is measured in reference to the valence band-top (VBT) energy. Brief description is as follows. A stainless-steel sample holder was filled with a titania powder sample and set in a home-made photoacoustic (PA) cell equipped with an electret condenser microphone and a quartz window on the upper side. The PA cell was filled with methanol-saturated argon, and two light beams were introduced simultaneously using a UV quartz combiner light guide (Moritex MWS5-1000S-UV3). One was a 625-nm light beam from an LED modulated by a digital function generator (NF Corporation DF1906) at 80 Hz, and the other was continuous monochromatic light from a monochromator (Spectral Products CM110 1/8m with a Spectral Products ASB-XE-175 xenon lamp) with a wavelength scanning from 650 nm to 350 nm with 5-nm steps. The raw spectrum obtained was differentiated from the lower-energy side and calibrated with the reported total electron-trap density in units of $\mu\text{mol}\cdot\text{g}^{-1}$ measured by a photochemical method to obtain an ERDT pattern. Using the same PAS cell, an ordinary single-beam PA spectrum was also measured to evaluate band gap, i.e., conduction band-bottom (CBB) energy in reference to VBT, of a sample. The thus-obtained ERDT and CBB were plotted as a function of energy from VBT.

4.3. Photocatalytic Decomposition of Acetaldehyde

Photocatalytic decomposition of acetaldehyde was carried out in a flow quartz tubular reactor of around 141 cm^3 in volume, placed in the thermostatic incubator with set temperature of 25°C . This reactor was surrounded with 3 ring-shaped lamps emitted visible light (L22W/840 Circular LUMILUX® Cool White) or UV (Philips, Eindhoven, The Netherlands, Special ‘TL’E 22W/10 Black Light). Gaseous acetaldehyde with concentration of 300 ppm in a dry air was flowing through the reactor from the supplied bottle with regulated flowing speed (5–50 mL/min) by an installed flow meter (El-Flow series, ZACH METALCHEM Company, Gliwice, Poland). The concentration of acetaldehyde was

monitored by a Gas Chromatograph SRI 8610C with FID detector set up behind the reactor, so outgoing gas from reactor was flowing through the dosing loop in a chromatograph and then was delivered to the CO₂ analyser (LAB-EL Company, Reguły, Poland, model LB-854) and wasted. The scheme of the installation set up was introduced in Figure 12. Photocatalyst sample was homogeneously spread on the surface of glass plates from its aqueous suspension, then was dried in oven for 1 h and placed inside the reactor. In total the surface of titania sample was 24 cm² (6 glass plates with dimension of 2 cm × 2 cm). The mass of sample coated glass plate was around 0.4 g. The emission spectra of applied lamps were showed in Figure 13.

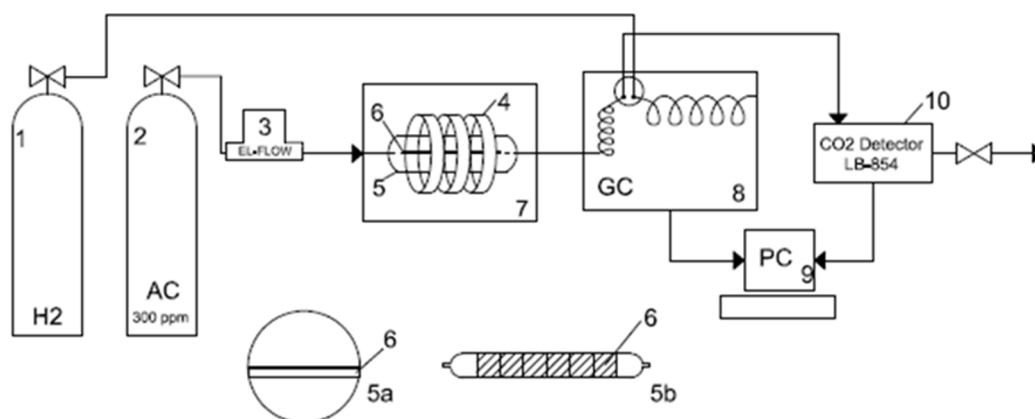


Figure 12. The scheme of the photocatalytic system; 1—bottle with H₂ carrier gas, 2—bottle with acetaldehyde (concentration of 300 ppm in a dry air), 3—flow meter (EL-Flow), 4—circular lamps, 5—quartz reactor: 5a—central view and 5b—top view, 6—glass plates with loaded sample, 7—incubator, 8—Gas Chromatograph (SRI 8610C), 9—Personal Computer (PC), 10—CO₂ detector (LB-854).

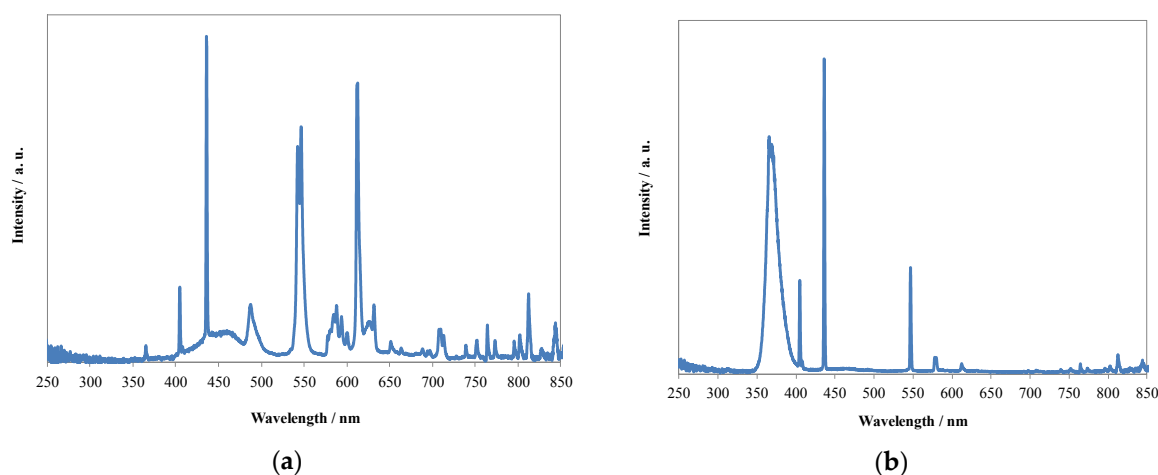


Figure 13. Emission spectra of lamps: (a) fluorescent, and (b) UV.

4.4. Photocatalytic Decomposition of Acetaldehyde

Activity of the prepared samples under visible light irradiation was measured by reaction of TA in an aqueous solution with OH radicals produced on the photocatalyst surface after its excitation. The formed product of reaction, 2-HTA was analyzed using fluorescence spectroscopy. As a source of visible light, halogen lamp of 150 W was applied with UV cut off filter ($\lambda > 425$ nm). The emission spectra of this lamp are illustrated in Figure 14.

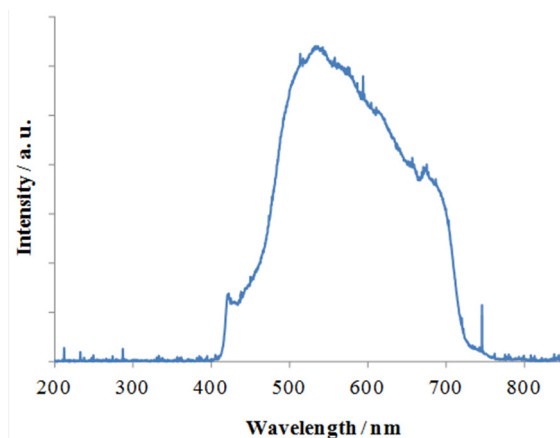


Figure 14. Emission spectrum of a halogen lamp with cut off filter ($\lambda > 425$).

Acknowledgments: Beata Tryba—wrote the manuscript, planned experiments, collected all the data and contributed in their interpretation, designed the photocatalytic test and partly performed the photocatalytic measurements; Magdalena Wozniak—did photocatalytic tests, UV-Vis/DR, FTIR and zeta potential measurements, contributed in analyses of data; Grzegorz Zolnierkiewicz—performed EPR analyses; Nikos Guskos—contributed in the analyses of EPR results; Antoni Morawski—support of the measurements of acetaldehyde decomposition; Christophe Colbeau-Justin—performed TRMC measurements and contributed in their analyses; Rafał Wrobel—performed and analysed XPS measurements; Akio Nitta—performed analyses of energy-resolved distribution of electron traps; Bunsho Ohtani—invented the method of electron traps measurements and contributed in the analyses of the obtained results.

Author Contributions: Beata Tryba conceived and designed the experiments. Magdalena Wozniak, Beata Tryba, Grzegorz Zolnierkiewicz, Rafał Wrobel, Christophe Colbeau-Justin and Akio Nitta performed experiments. Beata Tryba, Nikos Guskos, Rafał Wrobel and Bunsho Ohtani analyzed the data. Beata Tryba wrote the paper. Antoni Morawski supported construction of the photocatalytic system for acetaldehyde decomposition.

Conflicts of Interest: The authors declare no conflicts of interest.

References

1. Fujishima, A.; Zhang, X.; Tryk, A. TiO_2 photocatalysis and related surface phenomena. *Surf. Sci. Rep.* **2008**, *63*, 515–582. [[CrossRef](#)]
2. Meroni, D.; Ardizzone, S.; Cappelletti, G.; Oliva, C.; Ceotto, M.; Poelman, D.; Poelman, H. Photocatalytic removal of ethanol and acetaldehyde by N-promoted TiO_2 films: The role of the different nitrogen sources. *Catal. Today* **2011**, *161*, 169–174. [[CrossRef](#)]
3. Zhang, J.; Wu, Y.; Xing, M.; Leghari, S.A.K.; Sajjad, S. Development of modified N doped TiO_2 photocatalyst with metals, nonmetals and metal oxides. *Energy Environ. Sci.* **2010**, *3*, 715–726. [[CrossRef](#)]
4. Lin, Y.-H.; Weng, C.-H.; Tzeng, J.-H.; Lin, Y.-T. Adsorption and photocatalytic kinetics of visible-light response N-doped TiO_2 nanocatalyst for indoor acetaldehyde removal under dark and light conditions. *Intern. J. Photoen.* **2016**, *2016*, 1–9. [[CrossRef](#)]
5. Kitano, M.; Funatsu, K.; Matsuoka, M.; Ueshima, M.; Anpo, M. Preparation of nitrogen-substituted TiO_2 thin film photocatalysts by the radio frequency magnetron sputtering deposition method and their photocatalytic reactivity under visible light irradiation. *J. Phys. Chem. B* **2006**, *110*, 25266–25272. [[CrossRef](#)] [[PubMed](#)]
6. Dunnill, C.W.; Parkin, I.P. Nitrogen-doped TiO_2 thin films: Photocatalytic applications for healthcare environments. *Dalton Trans.* **2011**, *40*, 1635–1640. [[CrossRef](#)] [[PubMed](#)]
7. Miyauchi, M.; Ikezawa, A.; Tobimatsu, H.; Irie, H.; Hashimoto, K. Zeta potential and photocatalytic activity of nitrogen doped TiO_2 thin films. *Phys. Chem. Chem. Phys.* **2004**, *6*, 865–870. [[CrossRef](#)]
8. Etacheri, V.; Di Valentin, C.; Schneider, J.; Bahnemann, D.; Pillai, S.C. Visible-light activation of TiO_2 photocatalysts: Advances in theory and experiments. *J. Photochem. Photobiol. C* **2015**, *25*, 1–29. [[CrossRef](#)]
9. Kubacka, A.; Fernandez-García, M.; Colon, G. Advanced nanoarchitectures for solar photocatalytic applications. *Chem. Rev.* **2012**, *112*, 1555–1614. [[CrossRef](#)] [[PubMed](#)]

10. Asahi, R.; Morikawa, T.; Ohwaki, T.; Aoki, K.; Taga, Y. Visible-light photocatalysis in nitrogen-doped titanium oxides. *Science* **2001**, *293*, 269–271. [[CrossRef](#)] [[PubMed](#)]
11. Irie, H.; Watanabe, Y.; Hashimoto, K. Nitrogen-concentration dependence on photocatalytic activity of $\text{TiO}_{2-x}\text{N}_x$ powders. *J. Phys. Chem. B* **2003**, *107*, 5483–5486. [[CrossRef](#)]
12. Diwald, O.; Thompson, T.L.; Goralski, E.G.; Walck, S.D.; Yates, J.T. The effect of nitrogen ion implantation on the photoactivity of TiO_2 rutile single crystals. *J. Phys. Chem. B* **2004**, *108*, 52–57. [[CrossRef](#)]
13. Valentin, C.D.; Pacchioni, G.; Selloni, A.; Livraghi, S.; Giamello, E. Characterization of paramagnetic species in N-doped TiO_2 powders by EPR Spectroscopy and DFT calculations. *J. Phys. Chem. B* **2005**, *109*, 11414–11419. [[CrossRef](#)] [[PubMed](#)]
14. Ihara, T.; Miyoshi, M.; Iriyama, Y.; Matsumoto, O.; Sugihara, S. Visible-light-active titanium oxide photocatalyst realized by an oxygen-deficient structure and by nitrogen doping. *Appl. Catal. B* **2003**, *42*, 403–409. [[CrossRef](#)]
15. Sakatani, Y.; Nunoshige, J.; Ando, H.; Okusako, K.; Koike, H.; Takata, T.; Kondo, J.N.; Hara, M.; Domen, K. Photocatalytic decomposition of acetaldehyde under visible light irradiation over La^{3+} and N co-doped TiO_2 . *Chem. Lett.* **2003**, *32*, 1156–1157. [[CrossRef](#)]
16. Nitta, A.; Takase, M.; Takashima, M.; Murakami, N.; Ohtani, B. A fingerprint of metal-oxide powders: Energy-resolved distribution of electron traps. *Chem. Commun.* **2016**, *52*, 12096–12099. [[CrossRef](#)] [[PubMed](#)]
17. Colbeau-Justin, C.; Kunst, M.; Huguenin, D. Structural influence on charge-carrier lifetimes in TiO_2 powders studied by microwave absorption. *J. Mater. Sci.* **2003**, *38*, 2429–2437. [[CrossRef](#)]
18. Luna, A.L.; Novoseltceva, E.; Louarn, E.; Beaunier, P.; Kowalska, E.; Ohtani, B.; Valenzuela, M.A.; Remita, H.; Colbeau-Justin, C. Synergetic effect of Ni and Au nanoparticles synthesized on titania particles for efficient photocatalytic hydrogen production. *Appl. Catal. B* **2016**, *191*, 18–28. [[CrossRef](#)]
19. Chesalov, Y.A.; Chernobay, G.B.; Andrushkevich, T.V. FTIR study of the surface complexes of β -picoline, 3-pyridine-carbaldehyde and nicotinic acid on sulfated TiO_2 (anatase). *J. Mol. Catal. A* **2013**, *373*, 96–107. [[CrossRef](#)]
20. Yang, G.; Jiang, Z.; Shi, H.; Xiao, T.; Yan, Z. Preparation of highly visible-light active N-doped TiO_2 photocatalyst. *J. Mater. Chem.* **2010**, *20*, 5301–5309. [[CrossRef](#)]
21. Lopez, R.; Gomez, R. Band-gap energy estimation from diffuse reflectance measurements on sol-gel and commercial TiO_2 : A comparative study. *J. Sol-Gel Sci. Technol.* **2012**, *61*, 1–7. [[CrossRef](#)]
22. Biesinger, M.C.; Lau, L.W.M.; Gerson, A.R.; Smart, R.St.C. Resolving surface chemical states in XPS analysis of first row transition metals, oxides and hydroxides: Sc, Ti, V, Cu and Zn. *Appl. Surf. Sci.* **2010**, *257*, 887–898. [[CrossRef](#)]
23. Ketteler, G.; Yamamoto, S.; Bluhm, H.; Andersson, K.; Starr, D.E.; Ogletree, D.F.; Ogasawara, H.; Nilsson, A.; Salmeron, M. The nature of water nucleation sites on TiO_2 (110) surfaces revealed by ambient pressure X-ray photoelectron spectroscopy. *J. Phys. Chem. C* **2007**, *111*, 8278–8282. [[CrossRef](#)]
24. Diesen, V.; Dunnill, C.W.; Bear, J.C.; Firth, S.; Jonsson, M.; Parkin, I.P. Visible light photocatalytic activity in AACVD-prepared N-modified TiO_2 thin films. *Chem. Vap. Deposition* **2014**, *20*, 91–97. [[CrossRef](#)]
25. Quesada-Cabrera, R.; Sotelo Vazquez, C.; Darr, J.A.; Parkin, I.P. Critical influence of surface nitrogen species on the activity of N-doped TiO_2 thin-films during photodegradation of stearic acid under UV light irradiation. *Appl. Catal. B* **2014**, *160–161*, 582–588. [[CrossRef](#)]
26. Nolan, N.T.; Synnott, D.W.; Seery, M.K.; Hinder, S.J.; Van Wassenhovend, A.; Pillai, S.C. Effect of N-doping on the photocatalytic activity of sol-gel TiO_2 . *J. Hazard. Mater.* **2012**, *211–212*, 88–94. [[CrossRef](#)] [[PubMed](#)]
27. Cheng, X.; Yu, X.; Xing, Z.; Wan, J. Enhanced photocatalytic activity of nitrogen doped TiO_2 anatase nano-particle under simulated sunlight irradiation. *Energy Procedia* **2012**, *16*, 598–605. [[CrossRef](#)]
28. Dunnill, C.W.H.; Aiken, Z.A.; Pratten, J.; Wilson, M.; Morgan, D.J.; Parkin, I.P. Enhanced photocatalytic activity under visible light in N-doped TiO_2 thin films produced by APCVD preparations using t-butylamine as a nitrogen source and their potential for antibacterial films. *J. Photochem. Photobiol. A* **2009**, *207*, 244–253. [[CrossRef](#)]
29. Ohtani, B. Titania photocatalysis beyond recombination: A Critical Review. *Catalysts* **2013**, *3*, 942–953. [[CrossRef](#)]

30. Tryba, B.; Tygielska, M.; Colbeau-Justin, C.; Kusiak-Nejman, E.; Kapica-Kozar, J.; Wróbel, R.; Żołnierkiewicz, G.; Guskos, N. Influence of pH of sol-gel solution on phase composition and photocatalytic activity of TiO₂ under UV and visible light. *Mater. Res. Bull.* **2016**, *84*, 152–161. [[CrossRef](#)]



© 2018 by the authors. Licensee MDPI, Basel, Switzerland. This article is an open access article distributed under the terms and conditions of the Creative Commons Attribution (CC BY) license (<http://creativecommons.org/licenses/by/4.0/>).